ERJ Express. Published on October 25, 2018 as doi: 10.1183/13993003.00821-2018

EUROPEAN RESPIRATORY *journal*

FLAGSHIP SCIENTIFIC JOURNAL OF ERS

Early View

Original article

Patterns of regional lung physiology in cystic fibrosis using ventilation MRI and MBW

Laurie J. Smith, Guilhem J. Collier, Helen Marshall, Paul J.C. Hughes, Alberto M. Biancardi, Martin Wildman, Ina Aldag, Noreen West, Alex Horsley, Jim M. Wild

Please cite this article as: Smith LJ, Collier GJ, Marshall H, *et al*. Patterns of regional lung physiology in cystic fibrosis using ventilation MRI and MBW. *Eur Respir J* 2018; in press (https://doi.org/10.1183/13993003.00821-2018).

Patterns of regional lung physiology in cystic fibrosis using ventilation MRI and MBW

Authors: Laurie J. Smith[1,2], Guilhem J Collier[1], Helen Marshall[1], Paul JC Hughes[1], Alberto M. Biancardi[1], Martin Wildman[3], Ina Aldag[2], Noreen West[2], Alex Horsley[1,4], Jim M. Wild[1,5]

[1]*POLARIS, Academic Radiology, University of Sheffield, Sheffield, UK*

[2]*Sheffield Children's Hospital NHS Foundation Trust, Sheffield, UK*

[3]*Sheffield Teaching Hospital NHS Foundation Trust, Sheffield, UK*

[4]*Respiratory Research Group, Division of Infection, Immunity & Respiratory Medicine, University of Manchester, Manchester, UK*

[5]*Insigneo, Institute of in-silico medicine, Sheffield, UK*

Corresponding Author: Jim M. Wild. POLARIS, Academic Radiology, Department of Infection, Immunity & Cardiovascular Disease, University of Sheffield, Sheffield, UK. Telephone: + 44 (0)114 2159141. Email: j.m.wild@sheffield.ac.uk

Take home message: *Ventilation distribution on MRI improves at TLC and two distinct patterns of regional lung disease in CF are highlighted, where abnormal FEV_1 is associated with VDP >10%. Ventilation MRI & MBW are highly correlated*.

Glossary

CF – Cystic fibrosis

EIVt – End-inspiratory tidal volume

FEV_1 – Forced expiratory volume in 1 second

FRC -Functional residual capacity

^3He – Helium-3

LCI – Lung clearance index

MBW – Multiple breath washout

MRI – Magnetic resonance imaging

RV – Residual volume

S_{cond} – convection dependent ventilation heterogeneity

S_{acin} - convection-diffusion dependent ventilation heterogeneity

TCV – Thoracic cavity volume

TLC – Total lung capacity

VDP – Ventilation defect percentage

VH_I – Ventilation heterogeneity index

VV – Ventilated volume

Abstract

Hyperpolarised helium-3 (^{3}He) ventilation MRI and multiple-breath washout (MBW) are sensitive methods for detecting lung disease in cystic fibrosis (CF). We aimed to explore their relationship across a broad range of CF disease severity and patient age, as well as assess the effect of inhaled lung volume on ventilation distribution.

32 children and adults with CF underwent MBW and ^{3}He-MRI at a lung volume of end-inspiratory tidal volume (EIVt). 28 patients also performed ^{3}He-MRI at total lung capacity (TLC). ^{3}He-MRI were quantitatively analysed for; ventilation defect percentage (VDP), ventilation heterogeneity index (VH_I), and the number and size of individual contiguous ventilation defects. From MBW, the lung clearance index (LCI), S_{cond} and S_{acin} were calculated.

VDP and VH_I at EIVt strongly correlated with LCI (r=0.89,r=0.88 respectively), S_{acin} (r=0.84,r=0.82) and FEV_1 (r=-0.79,r=-0.78). Two distinct ^{3}He-MRI patterns were highlighted; patients with abnormal FEV_1 had significantly ($p<0.001$) larger, but fewer contiguous defects than those with normal FEV_1 who tended to have numerous small volume defects. These two MRI patterns were delineated by a VDP of approximately 10%. At TLC, when compared to EIVt, VDP and VH_I reduced in all subjects ($p<0.001$), demonstrating improved ventilation distribution and also regions of volume-reversible and non-reversible ventilation abnormalities.

Introduction

Hyperpolarised gas ventilation MRI allows for detailed and sensitive quantitative assessment of regional lung ventilation abnormalities in patients with obstructive airways disease [1-4]. The MRI technique usually involves the inhalation of a fixed volume of hyperpolarised noble gas and the resulting distribution of ventilation is imaged during a short breath-hold. In patients with cystic fibrosis (CF) it has been shown to be highly sensitive to detect early lung disease in children [5, 6], to track disease progression [7] and to assess treatment response [8]. The use of a fixed inhalation volume however, will result in patients with smaller lung volume being closer to their total lung capacity (TLC) than patients with larger lung volume. The effect that this has on the distribution of ventilation has not yet been assessed in CF. In addition, understanding the nature and pattern of regional ventilation defects seen on MRI, across the spectrum of CF lung disease, will allow for a greater understanding of lung disease pathophysiology and progression.

The lung clearance index (LCI), derived from multiple-breath washout (MBW) is a physiological measure of global ventilation heterogeneity that is sensitive to early lung disease [9]. LCI correlates with structural abnormalities seen on CT [10-12] and MRI [13] and is also sensitive to treatment response [14]. The utility of LCI in CF has been established primarily in children and patients with mild disease. In more severe CF lung disease, when previously obstructed regions open up to tidal ventilation due to treatment, the LCI response is unpredictable and may worsen despite improvements in FEV_1 [15-19]. Comparing LCI to ventilation MRI may therefore help to better understand ventilation abnormalities expressed by the two methods.

In this work we therefore aimed to:

(1) Compare ventilation MRI and MBW, including LCI and the phase III slope outcomes S_{cond} (convection dependent ventilation heterogeneity) and S_{acin} (convection-diffusion dependent ventilation heterogeneity), in children and adults with CF with a broad range of lung disease severity.

(2) Assess ventilation MRI at two different lung volumes in order to investigate the nature of reversible airway obstruction in CF.

(3) Assess the relationship between size and number of individual contiguous ventilation defects from ventilation MRI in CF patients across a broad range of disease severity to aid understanding of regional imaging data and disease status.

Methods

Children and adults with CF were recruited from three UK specialist centres (Sheffield Children's Hospital and Northern General Hospital, Sheffield, UK and Manchester Adult CF Centre, Manchester, UK). Patients were required to be aged over five years, be clinically stable for four weeks prior to their visit and achieve an FEV_1 >30% predicted within the previous six months. This study was approved by the Yorkshire and Humber - Leeds West Research Ethics Committee (REC reference: 16/YH/0339). Parents/guardians of children and all adult patients provided written informed consent.

MRI acquisition

Ventilation MRI was performed on a 1.5T GE HDx scanner (GE, Milwaukee, USA) using hyperpolarised helium-3 (^{3}He) using a transmit-receive vest coil (CMRS, Milwaukee, USA) and a 3D ventilation imaging sequence as described previously [20]. Images were acquired at two different lung inhalation volumes during separate breath-holds. Firstly, images were acquired at a lung volume corresponding to end-inspiratory tidal volume (EIVt), by inhaling a pre-determined fixed volume of test gas from their resting functional residual capacity (FRC). This corresponds to the approximate inspired volume most typically reported in studies to date [1, 5, 6, 8, 21-28]. The volume of gas was titrated based on the subject's height and consisted of scaled doses of ^{3}He and balanced with nitrogen (N_2) (E-Table 1). Secondly, images were acquired at TLC by repeating the EIVt-breathing manoeuvre, immediately followed by a full inhalation of room air. Further methodological details are described in the OLS.

MRI Post-Processing

For both the EIVt and TLC ^{3}He and ^{1}H image pairs, image metrics were calculated from a semi-automated segmentation [29]. The ^{3}He images were segmented in order to calculate the ventilated lung volume (VV) and the ^{1}H images were used to calculate the thoracic cavity volume (TCV). From these two segmentations the ventilation defect percentage (VDP) and the ventilation heterogeneity index (VH_I) were calculated (See Table 1 and OLS).

Contiguous individual ventilation defects in 3D were assessed. Defects that contributed to <1% of total VDP were discarded. The number of remaining defects ($N_{defects}$), as well as the volume of individual defects were calculated. The image analysis workflow is summarised in E-Figure 2.

To describe the degree of ventilation change from EIVt to TLC, the reversible-volume index was calculated from the EIVt and TLC images by:

$$\text{Reversible-volume index} = \frac{(\Delta VV)}{(\Delta TCV)}$$

Where $\Delta VV = VV_{(TLC)} - VV_{(EIVt)}$ and $\Delta TCV = TCV_{(TLC)} - TCV_{(EIVt)}$. Finally, the difference in VH_I (ΔVH_I) was quantified by: $\Delta VH_I = VH_{I\,(TLC)} - VH_{I\,(EIVT)}$.

Pulmonary Function

MBW was performed as previously described using a modified open-circuit Innocor and 0.2% SF_6 [30]. MBW was performed in triplicate both seated and supine [31]. From MBW, the metrics; lung clearance index (LCI), S_{cond} and S_{acin} were calculated and the average taken from at least two technically acceptable trials. Spirometry and body plethysmography were performed to international standards [32, 33] using a 'PFT Pro' (Vyaire, Basingstoke, UK) and recommended reference equations [34]. All tests were performed on the same day. Either MBW or MRI was performed first, followed by the other. Spirometry was always performed last.

Statistical analysis

Metrics were assessed for normality using the Shapiro-Wilks test and expressed as either the mean (SD) or the median (range). Patients were grouped into three groups; group 1 consisted of patients with normal FEV_1 (>-1.64 z-score) and normal LCI (<7.4 [30]); group 2 had normal FEV_1 but abnormal LCI (≥7.4); and group 3 had both abnormal FEV_1 and LCI. Group comparisons were assessed using the Kruskal-Wallis with Dunn's multiple comparisons test. As a result of this analysis, two refined groups are referred to throughout the results; those with normal FEV_1 (z-score >-1.64) and those with abnormal FEV_1 (z-score ≤-1.64). Spearman's correlation analysis was performed to assess the relationship between metrics. In total 13 metrics were considered, therefore after Bonferroni adjustment [35], a p-value <0.004 was considered significant for correlation analysis. The Wilcoxon-signed rank test was used to assess the difference in MRI metrics between EIVt and TLC. All analyses were performed in GraphPad Prism (V7.0, San Diego, US).

Results

32 patients with CF were recruited and assessed (17 (53%) female). Patient demographics, lung function and MRI metrics are presented in Table 2. Of the 32 patients studied, all but one child had visible ventilation abnormalities on ventilation MRI at EIVt. E-Figure 4 shows representative ^{3}He images for all patients. 30 patients (94%) had a VDP >2% at EIVt, the upper value from healthy controls previously reported [6]. In contrast, 26 (81%) patients had raised LCI and 14 (44%) patients had abnormal FEV_1. This resulted in six patients with normal FEV_1 and LCI (Group 1), 12 patients with normal FEV_1 but abnormal LCI (Group 2) and 14 patients with abnormal FEV_1 and LCI (Group 3). At EIVt, group 3 had significantly higher VDP, VH_I, largest individual defect and a significantly lower total number of individual defects ($p<0.001$), than groups 1 and 2. There was however no significant difference between groups 1 and 2 for these metrics, though a trend towards higher VH_I was seen in group 2 (Figure 1). The only metric to significantly distinguish groups 1 and 2 was S_{cond} ($p=0.03$).

Figure 2 demonstrates 3D ventilation MR images at EIVt with contiguous ventilation defects highlighted, examples shown are for a patient in group 2 and a patient in group 3.

Correlations between lung function and MRI at EIVt

VDP demonstrated significant correlation ($p<0.001$, Figure 3) with: LCI ($r=0.89$) and S_{acin} ($r=0.84$), but not S_{cond} ($r=0.32$); VDP also correlated with RV/TLC ($r=0.80$) and FEV_1 ($r=-0.79$). VH_I demonstrated significant correlations with LCI ($r=0.88$) and S_{acin} ($r=0.82$), but not S_{cond} ($r=0.46$ E-Figure 5); and with RV/TLC ($r=0.78$) and FEV_1 ($r=-0.78$). Supine MBW results also demonstrated significant equivalent correlations and are documented in E-Table 2.

The volume of the largest defect correlated significantly ($p<0.001$) with VDP ($r=0.97$, Figure 4), LCI ($r=0.85$), FEV_1 ($r=-0.80$) and S_{acin} ($r=0.79$) and the number of defects demonstrated a significant correlation with VDP ($r=-0.86$), LCI (-0.75), FEV_1 ($r=0.75$) and S_{acin} ($r=-0.62$).

Ventilation MRI comparison between EIVt and TLC

Ventilation images at both EIVt and TLC were successfully acquired from 28 patients (Table 3). Two patients were excluded due to acquisition errors and two patients could not successfully coordinate the TLC breathing manoeuvre. The median (range) TCV measured from ^{1}H MRI at EIVt was 78.2 (61.2,95.0)% of the TCV at TLC, which was significantly correlated to the FRC_{pleth}/TLC ratio (a marker of lung hyperinflation) measured during body plethysmography (r=0.68). The TCV at TLC was 97.7 (85.0,107.7)% of the TLC measured during body plethysmography.

At TLC there was a marked reduction in ventilation abnormalities. Signal intensity in ventilated regions of the lungs appeared more homogeneous, and in most patients some areas of un-ventilated lung became ventilated at TLC. This resulted in fewer ventilation defects at TLC for some patients whilst in others ventilation abnormalities remained (Figure 5). At TLC when compared to EIVt, there was a significant decrease ($p<0.001$, Figure 6) in MRI markers (expressed as median difference [95% confidence interval]) including: VDP -4.7 [-11.0,-2.2]%; VH_I -4.1 [-5.6,-3.1]%; volume of the largest defect -47.3 [-160.1, -17.1]mL, and largest defect expressed as a percentage of TCV -1.7 [-4.3,-0.8]%. 10/28 patients had a reduction in $N_{defects}$ at TLC (p=0.2), all of whom had normal FEV_1. The reversible-volume index, but not ΔVH_I, significantly correlated with VDP at EIVt (r=0.85) and with LCI (r=0.82, E-Figure 6), S_{acin} (r=0.75) and FEV_1 (r=-0.74). The reversible-volume index was significantly higher in group 3 than in groups 1 and 2 ($p<0.001$), but not between groups 1 and 2. ΔVH_I was not significantly different between groups.

VDP at TLC significantly correlated with LCI (r=0.85), S_{acin} (r=0.77), FEV_1 (r=-0.79) and RV/TLC (r=0.86). VH_I at TLC significantly correlated with LCI (r=0.82), S_{acin} (r=0.74), FEV_1 (r=-0.84) and RV/TLC (r=0.86).

Discussion

In this study we present a detailed analysis of the relationship between MBW and hyperpolarised gas ventilation MRI in patients with CF, across a broad range of age and disease severity. This analysis

confirms the strong relationships between global MRI and MBW metrics that have previously been reported in smaller cohort studies, performed across narrower ranges of age and disease severity [5-7]. Previous work has documented that patients with CF have ventilation defects evident on hyperpolarised gas MRI [1, 8, 21, 24, 36, 37], that the technique is reproducible and repeatable [21, 24] and that it can be used to assess regional response to treatment [8, 28]. Here we demonstrate what appear to be two distinct ventilation MRI patterns of CF lung disease; (i) patients who have numerous smaller defects (and normal FEV_1); and (ii), patients who have fewer but much larger contiguous defects, where FEV_1 is invariably reduced. We have also demonstrated that many of these ventilation abnormalities are lung volume dependent. When larger volumes are inhaled, some apparently obstructed airways open and allow gas to ventilate previously un-ventilated areas.

This last observation has important implications from an imaging methodology perspective. Studies utilising hyperpolarised gas are often performed by inhaling fixed gas volumes, with one litre of gas inhaled from FRC being common [21-25]. This however results in smaller subjects being closer to their TLC than taller subjects, potentially reducing VDP and making cross-sectional comparisons challenging. Recent paediatric studies have titrated the inhaled volume based on measured or predicted lung volume [6, 7, 26, 27] and we recommend this practice for all patients with CF. It is important to note however that we have not directly compared the inhaled volume given in this study to a fixed 1 litre inhalation.

The finding that only some ventilation defects decrease in size at TLC implies that regions of volume-reversible airways obstruction and regions of complete airways obstruction (that are fixed on the time-scale of the imaging session) co-exist in CF lungs. The reversibility of defects with deep inhalation highlights the probable value of physiotherapy and exercise in opening these lung regions, and also the potential for ventilation MRI to aid targeted therapies to be applied to specific lung regions. The change in ventilation from EIVt to TLC was not uniform across the population, with some patient's ventilation remaining distinctly abnormal at TLC. Assessing the transient nature of these lung-volume dependent ventilation defects longitudinally may provide insight into the progression of disease pathophysiology.

The analysis of contiguous ventilation defects allows quantification and tracking of individual defects over time. Two distinct ventilation MRI patterns at EIVt are highlighted, which may represent different ends of the disease spectrum in CF. Figure 4 demonstrates that in those patients with normal FEV_1, VDP is <10% and predominantly consists of numerous small-volume defects (possibly due to predominantly peripheral airways disease), which also appear more likely to be reversible. By the time FEV_1 becomes abnormal however, VDP is invariably >10%. In these patients, VDP is dominated by fewer larger contiguous defects (suggesting widespread airways disease and lobar destruction), possibly in part due to smaller defects merging with disease progression. In addition, these larger defects are less likely to disappear with full inspiration, suggesting a significant proportion of peripheral lung is not being routinely ventilated during tidal breathing. Such regions are likely to harbour reservoirs of trapped mucus and inflammatory exudate, encouraging further lung inflammation and damage. These findings in part are in contrast to previous work [37-39], which reported that the number of ventilation defects increased with worsening lung disease. This is likely due to the two dimensional (2D) assessment of ventilation images in previous studies, resulting in individual defects that span multiple slices being classed as multiple defects. Whereas in this 3D assessment of ventilation defects, defects are shown to be contiguous and not independent between slices, resulting in fewer individual defects.

There is an intuitive relationship between ventilation MRI and MBW metrics, as they both assess the distribution of inhaled gas within the lungs. These data suggest this relationship is stronger when MRI was performed at EIVt when compared to TLC, due to the EIVt manoeuvre most closely representing the end-inspiratory cycle of quiet breathing performed during MBW. Ventilation MRI has the advantage that the exact regional nature of this ventilation distribution can be assessed, including lung regions that are entirely blocked (and hence silent to MBW testing). In this cohort we found that LCI and S_{acin} had strong relationships with VDP and VH_I and also with reversible-volume index. S_{cond} however showed poor correlations due to the 'plateau effect' evident in E-figure 5, which occurs with increasing disease. This plateau has been reported previously [40], and suggests S_{cond} is useful primarily as a marker of very early CF lung disease, highlighted by the finding that S_{cond} was the only metric to significantly differentiate between groups 1 and 2. Convection-dependent ventilation heterogeneity therefore seems to be an early event in disease progression. Figure 3 suggests a

similar relationship may be evident when comparing LCI and VH_I, albeit the plateau effect for VH_I occurs at much higher levels of LCI. Up to this point, VH_I is strongly associated with increasing LCI. It is possible that with increasing lung disease in an individual, areas of increased VH_I become non-ventilated and contribute directly to VDP instead.

Higher values for the reversible-volume index indicate that a greater proportion of EIVt ventilation defects receive ventilation at TLC, implying volume-reversible airway obstruction. Reversible-volume index showed significant correlations with both LCI and S_{acin}. We hypothesise that this positive correlation may indicate that ventilation defects present at EIVt, which become ventilated at TLC, may be lung regions responsible for delayed gas washout during MBW. On the other hand, patients with large VDP but relatively low LCI may be explained by the presence of defects that are unable to achieve ventilation at TLC (i.e. low reversible-volume index), therefore these defects may not significantly contribute to the dynamic LCI signal (E-figures 6 and 7). The reversible-volume index may therefore help explain why an unpredictable LCI response is seen with treatments in more severe and acute CF lung disease, despite clinical and spirometric improvements. We postulate that a lower reversible-volume index in a subject with significant ventilation abnormalities will result in a relatively low LCI for their level of lung disease (E-figure 7). In response to treatment, we hypothesise that both the reversible-volume index and the LCI would increase in this case, caused by the opening of previously blocked lung regions to the MBW signal.

There are limitations to this study that require consideration. Whilst we have reported large numbers of patients for a ventilation MRI study [1, 5, 6, 8, 21, 22, 26, 27, 36, 37], there are still relatively small numbers of subjects in each sub-group, which inevitably limits the generalizability of this comparison. In comparing ventilation MRI with MBW we also acknowledge that the inert gases used have different diffusivity within the lung. ^{3}He has higher diffusivity in air when compared to SF_6, suggesting SF_6 may reveal larger ventilation defects if used in MR imaging. This has been reported when comparing ^{3}He with ^{129}Xe ventilation imaging in COPD [41]. A limitation of the individual defect analysis is that it assesses contiguous areas of signal void within the ventilation images, which are not necessarily anatomically contiguous. The larger defects evident in more severe disease can in some cases be seen to merge across different lung lobes which are fed by distinct conducting airways and therefore do not

represent a physiologically discrete defect caused by blockage of a single airway. Finally, in order to validate these cross-sectional findings, longitudinal data are required to determine whether the different patterns of ventilation observed behave as we predict on an individual basis over time.

In conclusion, this work adds to a growing body of work highlighting the use of ventilation MRI in CF, and specifically the role of VDP as a potential clinical tool and endpoint in clinical trials. In particular two key novel aspects are highlighted that help define the clinical meaning and utility of the methodology. Firstly, we highlight a VDP value of 10%, which separates normal and abnormal FEV_1 values, (the current clinical gold standard) and also appears to delineate a boundary between the two distinct ventilation imaging patterns described, i.e. numerous small defects versus fewer large defects. Secondly, we demonstrate the coexistence of reversible and non-reversible regions of airway obstruction in CF using ventilation imaging at different lung volumes. This has direct impact on the longitudinal monitoring of an individual's lung health and delivery of regionally specific treatment.

Acknowledgements

The authors would like to acknowledge all members of the POLARIS research group at the University of Sheffield for the support. In particular we would like to thank Mrs Leanne Armstrong for administrative support, Mr Jody Bray for assisting with MRI scanning, Mr Oliver Rodgers for polarisation of ^3He during MRI and Dr Chris Johns for reviewing all images. We would also like to thank the Cystic Fibrosis clinical teams at Sheffield Children's Hospital, Sheffield Teaching Hospital and Manchester CF Centre for their support. Finally we would like to thank all of the participants for their time in taking part in this research.

Financial Support

This report is independent research supported by the National Institute for Health Research and Health Education England and also the Medical Research Council. The views expressed in this publication are those of the author(s) and not necessarily those of the NHS, the National Institute for Health Research, Health Education England or the Department of Health.

References

1. McMahon, C.J., J.D. Dodd, C. Hill, N. Woodhouse, J.M. Wild, S. Fichele, C.G. Gallagher, S.J. Skehan, E.J. van Beek, and J.B. Masterson, *Hyperpolarized 3helium magnetic resonance ventilation imaging of the lung in cystic fibrosis: comparison with high resolution CT and spirometry.* Eur Radiol, 2006. **16**(11): p. 2483-90.
2. Kirby, M., S. Svenningsen, A. Owrangi, A. Wheatley, A. Farag, A. Ouriadov, G.E. Santyr, R. Etemad-Rezai, H.O. Coxson, D.G. McCormack, and G. Parraga, *Hyperpolarized 3He and 129Xe MR imaging in healthy volunteers and patients with chronic obstructive pulmonary disease.* Radiology, 2012. **265**(2): p. 600-10.
3. Svenningsen, S., F. Guo, D.G. McCormack, and G. Parraga, *Noncystic Fibrosis Bronchiectasis: Regional Abnormalities and Response to Airway Clearance Therapy Using Pulmonary Functional Magnetic Resonance Imaging.* Acad Radiol, 2017. **24**(1): p. 4-12.
4. Svenningsen, S., M. Kirby, D. Starr, H.O. Coxson, N.A. Paterson, D.G. McCormack, and G. Parraga, *What are ventilation defects in asthma?* Thorax, 2014. **69**(1): p. 63-71.
5. Kanhere, N., M.J. Couch, K. Kowalik, B. Zanette, J.H. Rayment, D. Manson, P. Subbarao, F. Ratjen, and G. Santyr, *Correlation of Lung Clearance Index with Hyperpolarized (129)Xe Magnetic Resonance Imaging in Pediatric Subjects with Cystic Fibrosis.* Am J Respir Crit Care Med, 2017. **196**(8): p. 1073-1075.
6. Marshall, H., A. Horsley, C.J. Taylor, L. Smith, D. Hughes, F.C. Horn, A.J. Swift, J. Parra-Robles, P.J. Hughes, G. Norquay, N.J. Stewart, G.J. Collier, D. Teare, S. Cunningham, I. Aldag, and J.M. Wild, *Detection of early subclinical lung disease in children with cystic fibrosis by lung ventilation imaging with hyperpolarised gas MRI.* Thorax, 2017. **72**(8): p. 760-762.
7. Smith, L., H. Marshall, I. Aldag, F. Horn, G. Collier, D. Hughes, N. West, A. Horsley, C.J. Taylor, and J. Wild, *Longitudinal Assessment of Children with Mild Cystic Fibrosis Using Hyperpolarized Gas Lung Magnetic Resonance Imaging and Lung Clearance Index.* Am J Respir Crit Care Med, 2018. **197**(3): p. 397-400.
8. Altes, T.A., M. Johnson, M. Fidler, M. Botfield, N.J. Tustison, C. Leiva-Salinas, E.E. de Lange, D. Froh, and J.P. Mugler, 3rd, *Use of hyperpolarized helium-3 MRI to assess response to ivacaftor treatment in patients with cystic fibrosis.* J Cyst Fibros, 2017. **16**(2): p. 267-274.
9. Aurora, P., P. Gustafsson, A. Bush, A. Lindblad, C. Oliver, C.E. Wallis, and J. Stocks, *Multiple breath inert gas washout as a measure of ventilation distribution in children with cystic fibrosis.* Thorax, 2004. **59**(12): p. 1068-73.
10. Gustafsson, P.M., P.A. De Jong, H.A. Tiddens, and A. Lindblad, *Multiple-breath inert gas washout and spirometry versus structural lung disease in cystic fibrosis.* Thorax, 2008. **63**(2): p. 129-34.
11. Owens, C.M., P. Aurora, S. Stanojevic, A. Bush, A. Wade, C. Oliver, A. Calder, J. Price, S.B. Carr, A. Shankar, J. Stocks, and C. London Cystic Fibrosis, *Lung*

Clearance Index and HRCT are complementary markers of lung abnormalities in young children with CF. Thorax, 2011. **66**(6): p. 481-8.
12. Ramsey, K.A., T. Rosenow, L. Turkovic, B. Skoric, G. Banton, A.M. Adams, S.J. Simpson, C. Murray, S.C. Ranganathan, S.M. Stick, G.L. Hall, and C.F. Arest, *Lung Clearance Index and Structural Lung Disease on Computed Tomography in Early Cystic Fibrosis.* Am J Respir Crit Care Med, 2016. **193**(1): p. 60-7.
13. Stahl, M., M.O. Wielputz, S.Y. Graeber, C. Joachim, O. Sommerburg, H.U. Kauczor, M. Puderbach, M. Eichinger, and M.A. Mall, *Comparison of Lung Clearance Index and Magnetic Resonance Imaging for Assessment of Lung Disease in Children with Cystic Fibrosis.* Am J Respir Crit Care Med, 2017. **195**(3): p. 349-359.
14. Amin, R., P. Subbarao, W. Lou, A. Jabar, S. Balkovec, R. Jensen, S. Kerrigan, P. Gustafsson, and F. Ratjen, *The effect of dornase alfa on ventilation inhomogeneity in patients with cystic fibrosis.* Eur Respir J, 2011. **37**(4): p. 806-12.
15. Pfleger, A., M. Steinbacher, G. Schwantzer, E. Weinhandl, M. Wagner, and E. Eber, *Short-term effects of physiotherapy on ventilation inhomogeneity in cystic fibrosis patients with a wide range of lung disease severity.* J Cyst Fibros, 2015. **14**(5): p. 627-31.
16. Welsh, L., C. Nesci, H. Tran, M. Tomai, and S. Ranganathan, *Lung clearance index during hospital admission in school-age children with cystic fibrosis.* J Cyst Fibros, 2014. **13**(6): p. 687-91.
17. Horsley, A.R., J.C. Davies, R.D. Gray, K.A. Macleod, J. Donovan, Z.A. Aziz, N.J. Bell, M. Rainer, S. Mt-Isa, N. Voase, M.H. Dewar, C. Saunders, J.S. Gibson, J. Parra-Leiton, M.D. Larsen, S. Jeswiet, S. Soussi, Y. Bakar, M.G. Meister, P. Tyler, A. Doherty, D.M. Hansell, D. Ashby, S.C. Hyde, D.R. Gill, A.P. Greening, D.J. Porteous, J.A. Innes, A.C. Boyd, U. Griesenbach, S. Cunningham, and E.W. Alton, *Changes in physiological, functional and structural markers of cystic fibrosis lung disease with treatment of a pulmonary exacerbation.* Thorax, 2013. **68**(6): p. 532-9.
18. Robinson, P.D., P. Cooper, P. Van Asperen, D. Fitzgerald, and H. Selvadurai, *Using index of ventilation to assess response to treatment for acute pulmonary exacerbation in children with cystic fibrosis.* Pediatr Pulmonol, 2009. **44**(8): p. 733-42.
19. Gozal, D., S.L. Bailey, and T.G. Keens, *Evolution of pulmonary function during an acute exacerbation in hospitalized patients with cystic fibrosis.* Pediatr Pulmonol, 1993. **16**(6): p. 347-53.
20. Horn, F.C., B.A. Tahir, N.J. Stewart, G.J. Collier, G. Norquay, G. Leung, R.H. Ireland, J. Parra-Robles, H. Marshall, and J.M. Wild, *Lung ventilation volumetry with same-breath acquisition of hyperpolarized gas and proton MRI.* NMR Biomed, 2014. **27**(12): p. 1461-7.
21. Kirby, M., S. Svenningsen, H. Ahmed, A. Wheatley, R. Etemad-Rezai, N.A. Paterson, and G. Parraga, *Quantitative evaluation of hyperpolarized helium-3 magnetic resonance imaging of lung function variability in cystic fibrosis.* Acad Radiol, 2011. **18**(8): p. 1006-13.
22. Mentore, K., D.K. Froh, E.E. de Lange, J.R. Brookeman, A.O. Paget-Brown, and T.A. Altes, *Hyperpolarized HHe 3 MRI of the lung in cystic fibrosis:*

assessment at baseline and after bronchodilator and airway clearance treatment. Acad Radiol, 2005. **12**(11): p. 1423-9.
23. O'Sullivan, B., M. Couch, J.P. Roche, R. Walvick, S. Zheng, D. Baker, M. Johnson, M. Botfield, and M.S. Albert, *Assessment of repeatability of hyperpolarized gas MR ventilation functional imaging in cystic fibrosis.* Acad Radiol, 2014. **21**(12): p. 1524-9.
24. Paulin, G.A., S. Svenningsen, B.N. Jobse, S. Mohan, M. Kirby, J.F. Lewis, and G. Parraga, *Differences in hyperpolarized (3) He ventilation imaging after 4 years in adults with cystic fibrosis.* J Magn Reson Imaging, 2015. **41**(6): p. 1701-7.
25. Sun, Y., B.P. O'Sullivan, J.P. Roche, R. Walvick, A. Reno, D. Baker, J.K. Mansour, and M.S. Albert, *Using hyperpolarized 3He MRI to evaluate treatment efficacy in cystic fibrosis patients.* J Magn Reson Imaging, 2011. **34**(5): p. 1206-11.
26. Thomen, R.P., L.L. Walkup, D.J. Roach, Z.I. Cleveland, J.P. Clancy, and J.C. Woods, *Hyperpolarized (129)Xe for investigation of mild cystic fibrosis lung disease in pediatric patients.* J Cyst Fibros, 2017. **16**(2): p. 275-282.
27. Walkup, L.L., R.P. Thomen, T.G. Akinyi, E. Watters, K. Ruppert, J.P. Clancy, J.C. Woods, and Z.I. Cleveland, *Feasibility, tolerability and safety of pediatric hyperpolarized (129)Xe magnetic resonance imaging in healthy volunteers and children with cystic fibrosis.* Pediatr Radiol, 2016. **46**(12): p. 1651-1662.
28. Woodhouse, N., J.M. Wild, E.J. van Beek, N. Hoggard, N. Barker, and C.J. Taylor, *Assessment of hyperpolarized 3He lung MRI for regional evaluation of interventional therapy: a pilot study in pediatric cystic fibrosis.* J Magn Reson Imaging, 2009. **30**(5): p. 981-8.
29. Hughes, P.J.C., F.C. Horn, G.J. Collier, A. Biancardi, H. Marshall, and J.M. Wild, *Spatial fuzzy c-means thresholding for semiautomated calculation of percentage lung ventilated volume from hyperpolarized gas and (1) H MRI.* J Magn Reson Imaging, 2018. **47**(3): p. 640-646.
30. Horsley, A.R., P.M. Gustafsson, K.A. Macleod, C. Saunders, A.P. Greening, D.J. Porteous, J.C. Davies, S. Cunningham, E.W. Alton, and J.A. Innes, *Lung clearance index is a sensitive, repeatable and practical measure of airways disease in adults with cystic fibrosis.* Thorax, 2008. **63**(2): p. 135-40.
31. Smith, L.J., K.A. Macleod, G.J. Collier, F.C. Horn, H. Sheridan, I. Aldag, C.J. Taylor, S. Cunningham, J.M. Wild, and A. Horsley, *Supine posture changes lung volumes and increases ventilation heterogeneity in cystic fibrosis.* PLoS One, 2017. **12**(11): p. e0188275.
32. Miller, M.R., J. Hankinson, V. Brusasco, F. Burgos, R. Casaburi, A. Coates, R. Crapo, P. Enright, C.P. van der Grinten, P. Gustafsson, R. Jensen, D.C. Johnson, N. MacIntyre, R. McKay, D. Navajas, O.F. Pedersen, R. Pellegrino, G. Viegi, J. Wanger, and A.E.T. Force, *Standardisation of spirometry.* Eur Respir J, 2005. **26**(2): p. 319-38.
33. Wanger, J., J.L. Clausen, A. Coates, O.F. Pedersen, V. Brusasco, F. Burgos, R. Casaburi, R. Crapo, P. Enright, C.P. van der Grinten, P. Gustafsson, J. Hankinson, R. Jensen, D. Johnson, N. Macintyre, R. McKay, M.R. Miller, D. Navajas, R. Pellegrino, and G. Viegi, *Standardisation of the measurement of lung volumes.* Eur Respir J, 2005. **26**(3): p. 511-22.

34. Quanjer, P.H., S. Stanojevic, T.J. Cole, X. Baur, G.L. Hall, B.H. Culver, P.L. Enright, J.L. Hankinson, M.S. Ip, J. Zheng, J. Stocks, and E.R.S.G.L.F. Initiative, *Multi-ethnic reference values for spirometry for the 3-95-yr age range: the global lung function 2012 equations.* Eur Respir J, 2012. **40**(6): p. 1324-43.
35. Bland, M., *An Introduction to Medical Statistics*, in *An Introduction to Medical Statistics*. 2015, Oxford University Press: Oxford, United Kingdom. p. 124.
36. Koumellis, P., E.J. van Beek, N. Woodhouse, S. Fichele, A.J. Swift, M.N. Paley, C. Hill, C.J. Taylor, and J.M. Wild, *Quantitative analysis of regional airways obstruction using dynamic hyperpolarized 3He MRI-preliminary results in children with cystic fibrosis.* J Magn Reson Imaging, 2005. **22**(3): p. 420-6.
37. Bannier, E., K. Cieslar, K. Mosbah, F. Aubert, F. Duboeuf, Z. Salhi, S. Gaillard, Y. Berthezene, Y. Cremillieux, and P. Reix, *Hyperpolarized 3He MR for sensitive imaging of ventilation function and treatment efficiency in young cystic fibrosis patients with normal lung function.* Radiology, 2010. **255**(1): p. 225-32.
38. Altes, T.A., P.L. Powers, J. Knight-Scott, G. Rakes, T.A. Platts-Mills, E.E. de Lange, B.A. Alford, J.P. Mugler, 3rd, and J.R. Brookeman, *Hyperpolarized 3He MR lung ventilation imaging in asthmatics: preliminary findings.* J Magn Reson Imaging, 2001. **13**(3): p. 378-84.
39. de Lange, E.E., T.A. Altes, J.T. Patrie, J. Parmar, J.R. Brookeman, J.P. Mugler, 3rd, and T.A. Platts-Mills, *The variability of regional airflow obstruction within the lungs of patients with asthma: assessment with hyperpolarized helium-3 magnetic resonance imaging.* J Allergy Clin Immunol, 2007. **119**(5): p. 1072-8.
40. Horsley, A.R., K.A. Macleod, A.G. Robson, J. Lenney, N.J. Bell, S. Cunningham, A.P. Greening, P.M. Gustafsson, and J.A. Innes, *Effects of cystic fibrosis lung disease on gas mixing indices derived from alveolar slope analysis.* Respir Physiol Neurobiol, 2008. **162**(3): p. 197-203.
41. Stewart, N.J., H.F. Chan, P.J.C. Hughes, F.C. Horn, G. Norquay, M. Rao, D.P. Yates, R.H. Ireland, M.Q. Hatton, B.A. Tahir, P. Ford, A.J. Swift, R. Lawson, H. Marshall, G.J. Collier, and J.M. Wild, *Comparison of (3) He and (129) Xe MRI for evaluation of lung microstructure and ventilation at 1.5T.* J Magn Reson Imaging, 2018.

Figure Captions

Figure 1: Kruskal-Wallis group comparison for VDP, VH_I, number of defects and largest individual contiguous defect, calculated from ventilation MRI at EIVt. Group 1 have both normal FEV_1 and LCI. Group 2 have normal FEV_1 but abnormal LCI. Group 3 have abnormal FEV_1 and LCI. In all graphs, group 3 is significantly different when compared to groups 1 and 2 ($p<0.001$), but there was no statistically significant difference between groups 1 and 2.

Figure 2: Demonstrates representative ventilation images at EIVt from a patient from group 2 (top) and group 3 (bottom). For both patients, the first row is a 3D ventilation image and the second row is a 3D ventilation image with the segmented individual contiguous ventilation defects added in colour. The colours associated with defects are arbitrary, but each different colour represents a single different radiologically contiguous defect. For each patient the ventilation image is observed from various anatomical angles. The top patient has VDP = 5.4%, largest defect (pink) = 1.5% of the TCV, $N_{defects}$ = 18. LCI = 7.7, FEV_1 z-score = -0.5. The bottom patient has VDP = 45.0%, largest defect (red) = 26.8% of the TCV, $N_{defects}$ = 3, LCI = 14.9, FEV_1 z-score = -5.4.

Figure 3: Scatter plots of VDP (top row) and VH_I (bottom row), both performed at EIVt, against pulmonary function metrics, with Spearman correlation values ($p<0.001$ in all).

Figure 4: Scatter plots of the number of individual contiguous ventilation defects ($N_{defects}$, top row) and the size of the largest individual contiguous defect (bottom row) at EIVt; against VDP at EIVt, LCI and FEV_1. In each graph patients are divided into those with an FEV_1 z-score <-1.64 (closed circles), or >-1.64 (open circles). For FEV_1 the dashed line represents the lower limit of normal (-1.64) and for LCI the dashed line represents the upper limit of normal (7.4). All Spearman correlations have a p-value <0.001.

Figure 5: Representative ^{3}He ventilation MR images acquired at EIVt and TLC from three subjects, with representative ^{1}H MRI. Subject A: FEV_1 z-score = -0.5, LCI = 7.7, RV/TLC = 22.4%. This subject has ventilation defects present at EIVt (VDP=5.4%), which largely disappear at TLC

(VDP=0.4%), reversible-volume index = 1.2. Subject B: FEV_1 z-score = -3.7, LCI = 17.8, RV/TLC = 50.3%. This subject has ventilation defects present at EIVt (VDP=39.5%), some of which remain at TLC (VDP=18.2%), reversible-volume index = 2.0. Subject C: FEV_1 z-score = -1.1, LCI = 7.4, RV/TLC = 24.8%. This subject has ventilation defects present at EIVt (VDP=6.5%), which largely remain at TLC (VDP=5.3%) and therefore has a low reversible-volume index (1.0). The cause of part of the non-reversible ventilation can be seen in the left lung on the ^1H image where an area of significant mucus is present, corresponding to the ventilation defect seen on both EIVt and TLC ventilation images (see arrow).

Figure 6: A comparison of ventilation MRI metrics between EIVt and TLC. At TLC there was a significant reduction in: VDP, VH_l, and the largest individual contiguous defect ($p<0.001$). The number of defects declined only for some subjects with normal FEV_1 (10/28 patients).

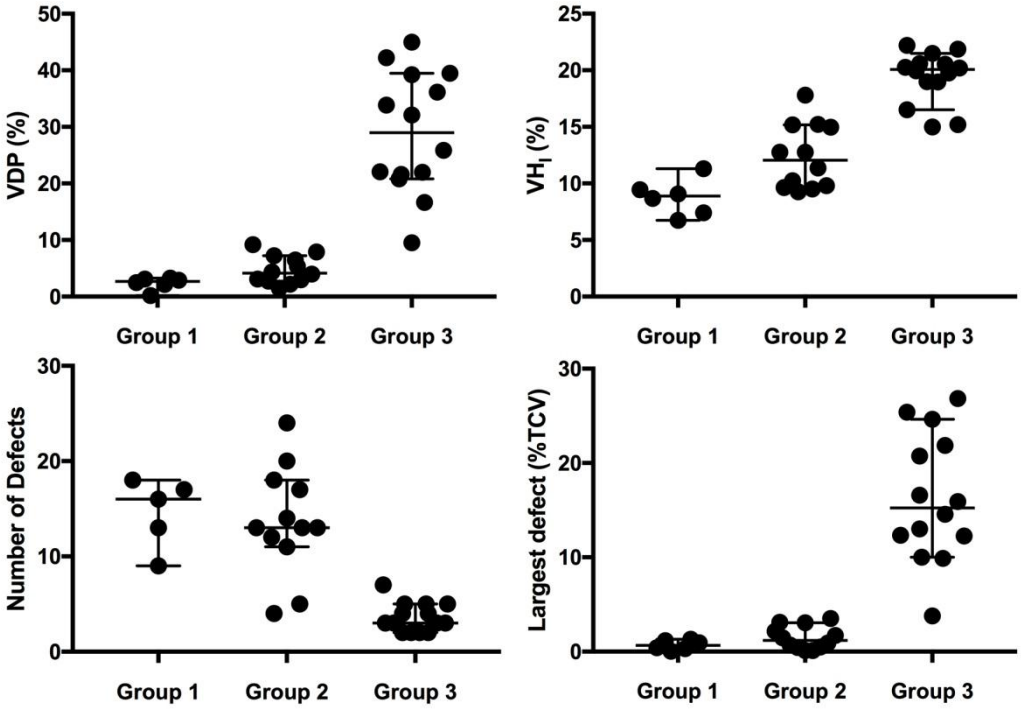
VDP (%)
50
40
30
20
10
0
Group 1
Group 2
Group 3
VH$_I$ (%)
25
20
15
10
5
0
Group 1
Group 2
Group 3
Number of Defects
30
20
10
0
Group 1
Group 2
Group 3
Largest defect (%TCV)
30
20
10
0
Group 1
Group 2
Group 3

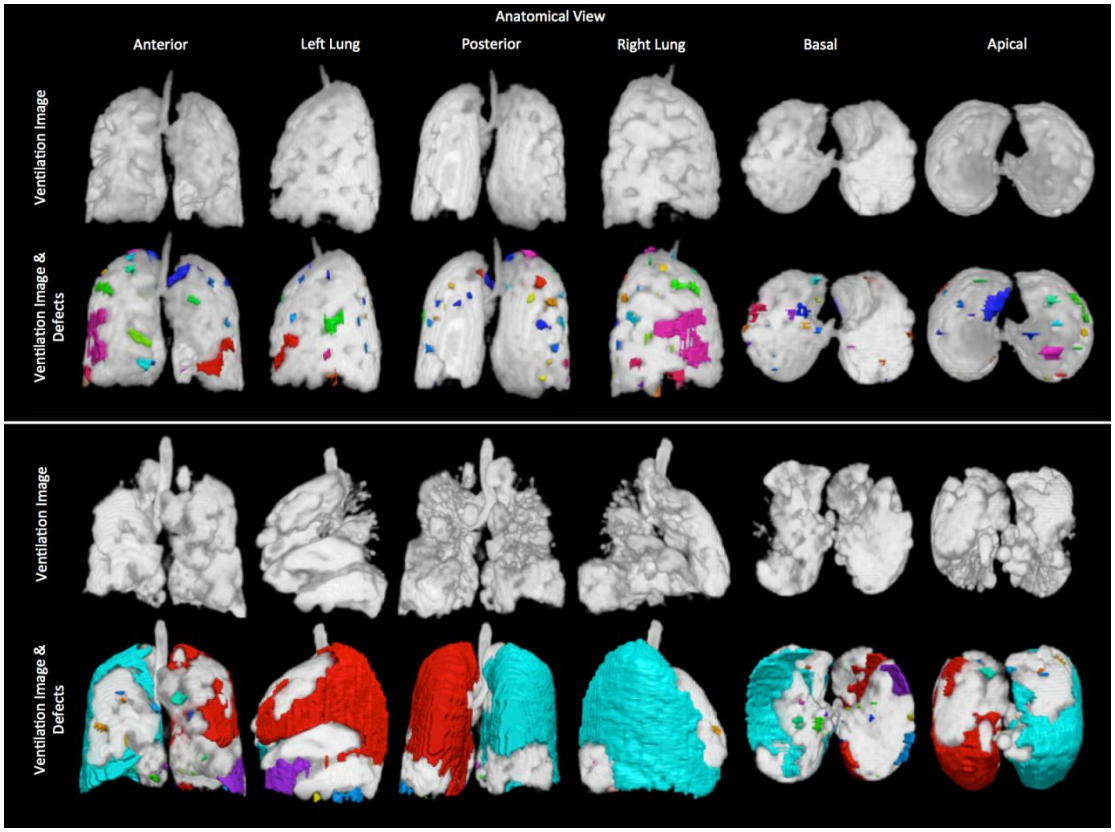
Anatomical View
Anterior
Left Lung
Posterior
Right Lung
Basal
Apical
Ventilation Image
Ventilation Image & Defects
Ventilation Image
Ventilation Image & Defects

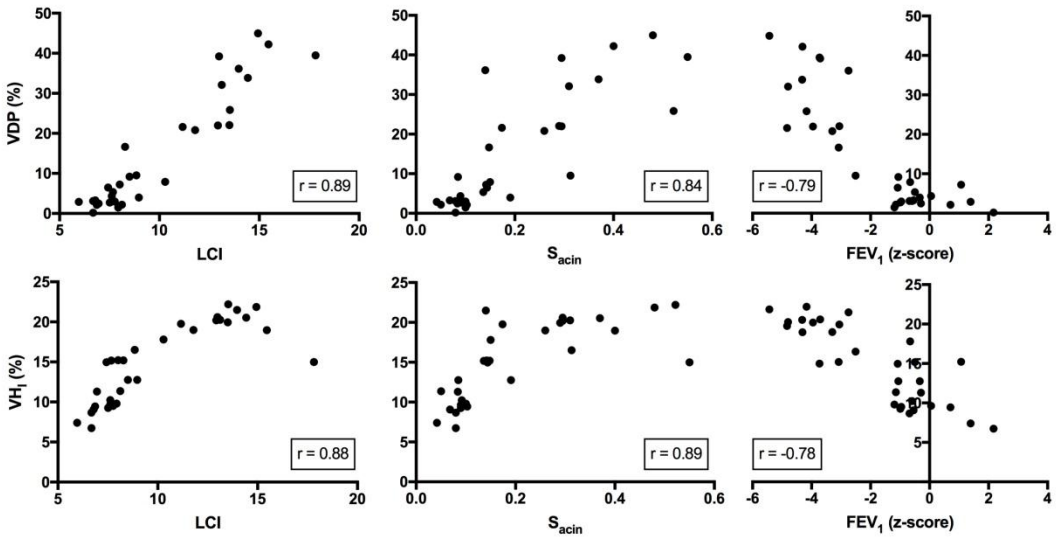
VDP (%)
LCI
r = 0.89
S_{acin}
r = 0.84
FEV_1 (z-score)
r = -0.79
VH_I (%)
LCI
r = 0.88
S_{acin}
r = 0.89
FEV_1 (z-score)
r = -0.78

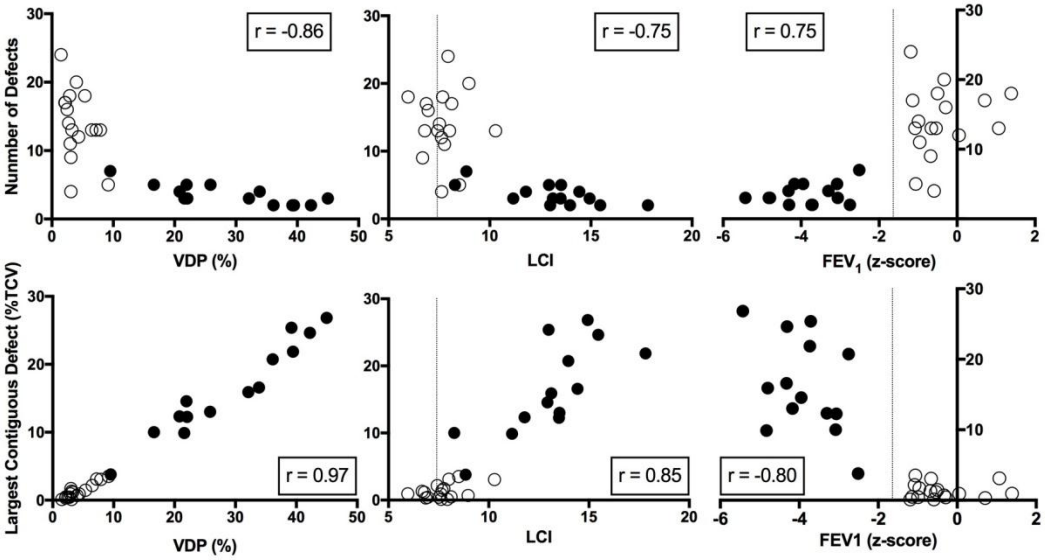
Nunmber of Defects
r = -0.86
r = -0.75
r = 0.75
VDP (%)
LCI
FEV1 (z-score)
Largest Contiguous Defect (%TCV)
r = 0.97
r = 0.85
r = -0.80
VDP (%)
LCI
FEV1 (z-score)

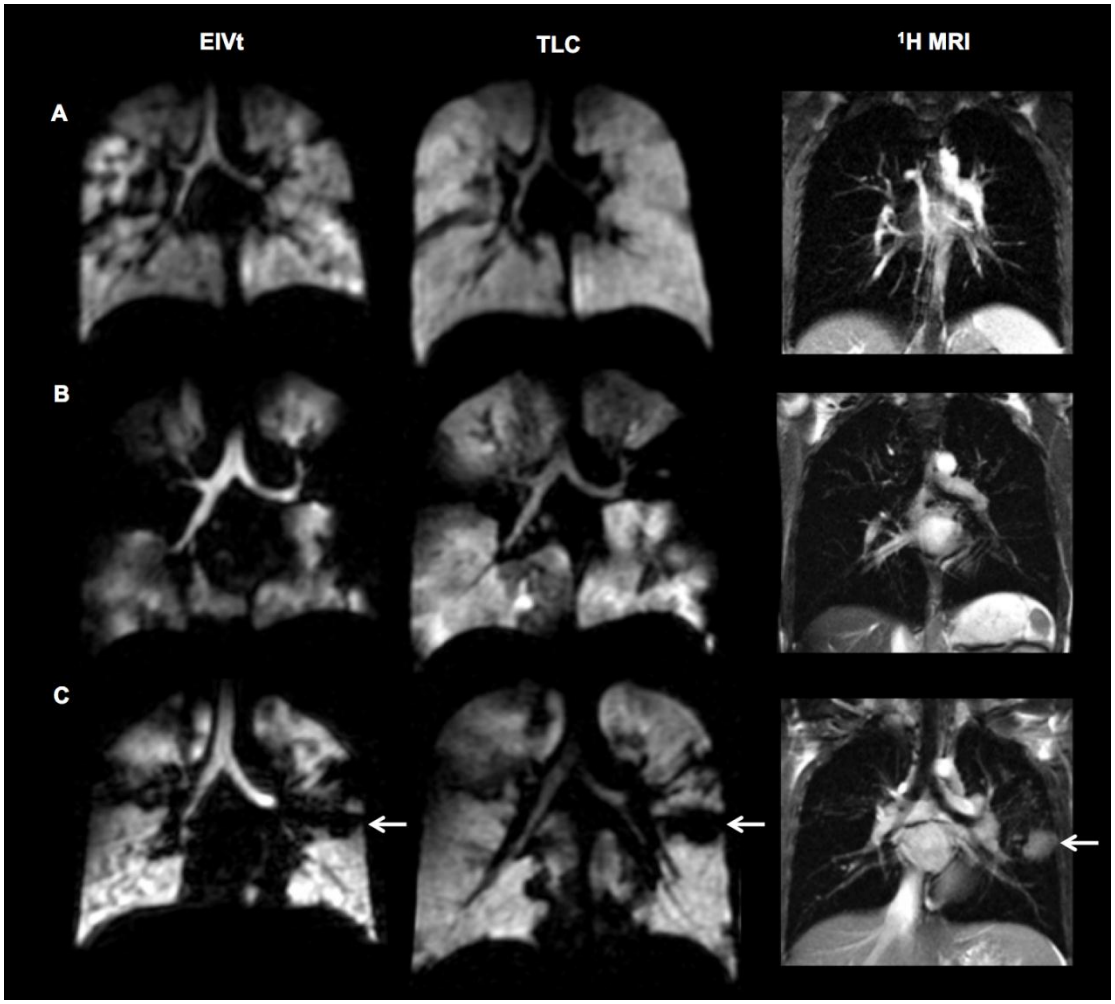
EIVt
TLC
^{1}H MRI
A
B
C

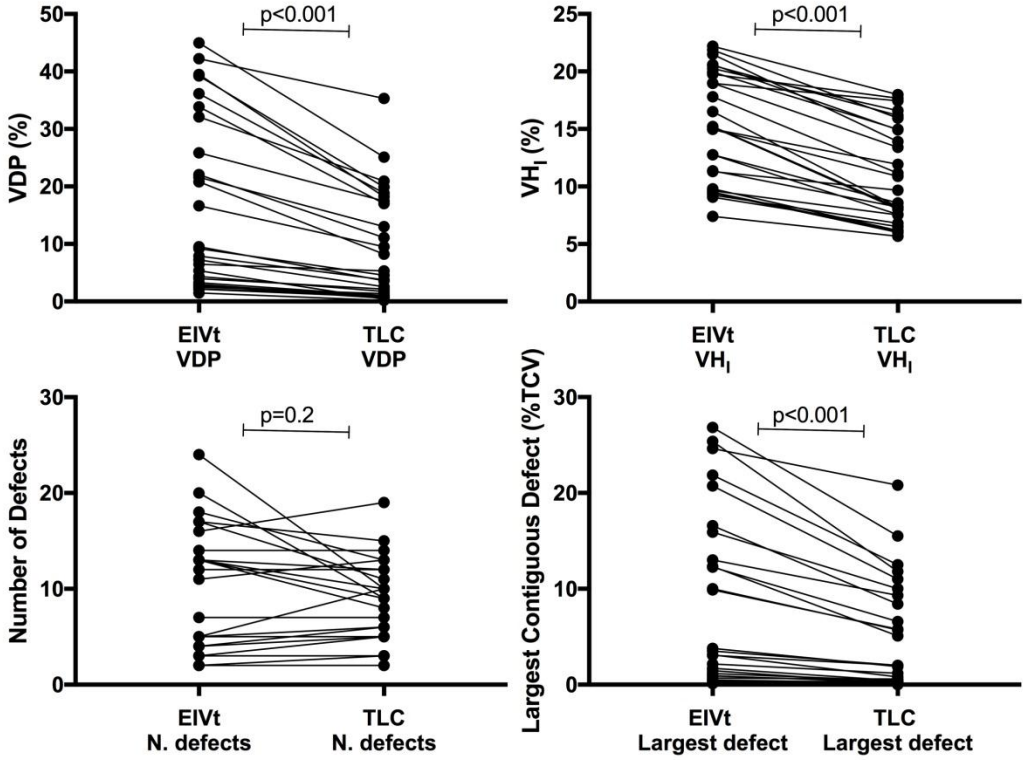
p<0.001
VDP (%)
50
40
30
20
10
0
EIVt
VDP
TLC
VDP
p<0.001
VHI (%)
25
20
15
10
5
0
EIVt
VHI
TLC
VHI
p=0.2
Number of Defects
30
20
10
0
EIVt
N. defects
TLC
N. defects
p<0.001
Largest Contiguous Defect (%TCV)
30
20
10
0
EIVt
Largest defect
TLC
Largest defect

Table 1: Description of metrics calculated from ^{3}He and ^{1}H MRI

Thoracic Cavity Volume (TCV)	Calculated from the segmentation of the ^{1}H anatomical MRI. The TCV is the lung volume at which ^{3}He-MRI is performed and is measured in litres.
Ventilated Volume (VV)	Calculated from ^{3}He ventilation image segmentation. VV represents the volume of ventilated lung and is measured in litres.
Ventilation Defect Percentage (VDP)	VDP is the percentage of the TCV that is not ventilated in the 3He MR images. Areas of the ^{3}He image that contribute to VDP appear black. It is calculated as: VDP = 100-((VV/TCV)*100). Larger VDP values are associated with increased lung disease.
Ventilation Heterogeneity Index (VH_I)	VH_I is a marker of the heterogeneity of the ^{3}He signal within ventilated regions of the ^{3}He MR images. For each ventilated pixel, a local coefficient of variation of signal intensity in the surrounding pixels is computed. VH_I is the inter-quartile range of the distribution of those values. Increased VH_I is associated with increased ventilation heterogeneity and therefore increased lung disease.
Number of ventilation defects ($N_{defects}$)	The number of individual 3D contiguous ventilation defects within the subject's lung. This only includes un-ventilated lung areas contributing to VDP. Defects were counted if the defect volume was >1% of total VDP.
Largest ventilation defect	This is the volume of the largest contiguous ventilation defect within the lungs. It is measured in litres and also as a percentage of the TCV.
Reversible-volume index	This represents the relative change that occurs in VV in response to the increase in TCV when comparing EIVt to TLC images. The reversible-volume index is equal to at least 1.0, the larger the value above 1.0 the greater the degree of EIVt ventilation defects that have resolved at TLC. In a healthy subject's lungs or in the lungs of a patient with non-reversible ventilation defects (resulting from complete obstruction), an increase in TCV due to deep inhalation, will result in equal increase in VV and the reversible-volume index will be 1. In contrast, any ventilation defect present at EIVt that at least partially resolves at TLC, will produce a reversible-volume index >1 (E-Figure 3).

Table 2: *Patient demographics, lung function and ventilation MRI metrics at End-inspiratory tidal volume (EIVt). Results are displayed for the whole population and for the three groups of patients. Group 1 = patients with normal spirometry and LCI. Group 2 = patients with normal spirometry but abnormal LCI and group 3 = abnormal spirometry and LCI. Metrics are presented as mean ± standard deviation (SD), or median (range) depending on the distribution of individual metrics.* FEV_1 *= forced expiratory volume in one second. RV/TLC = residual volume/total lung capacity. LCI = lung clearance index.* S_{cond} *= convection dependent ventilation heterogeneity.* S_{acin} *= convection-diffusion dependent ventilation heterogeneity. VDP = ventilation defect percentage.* VH_I *= ventilation heterogeneity index. TCV = thoracic cavity volume.* $N_{defects}$ *= number of defects. * denotes p<0.05 versus Group 1. ^ denotes p<0.05 versus Group 2.*

	Mean ± SD or Median (Range)			
	All patients	Group 1	Group 2	Group 3
N. (N. (%female))	32 (53%)	6	12	14
Age (years)	16.7 (6.4, 43.1)	10.1 (6.4, 16.5)	12.7 (8.3, 17.4)	29.9 (14.9, 43.1)*^
Height (cm)	156.2 ± 17.7	137.0 ± 16.1	153.7 ± 16.3	166.4 ± 11.7*
Weight (kg)	49.7 ± 18.4	32.8 ± 12.5	45.1 ± 15.1	60.9 ± 16.2*
FEV_1 (z-score)	-1.8 ± 2.03	0.5 ± 1.2	-0.6 ± 0.7	-3.9 ± 0.9*^
RV/TLC (%)	33.9 (17.8, 52.6)	23.5 (19.9, 26.5)	24.9 (17.8, 35.3)	47.7 (31.6, 52.6)*^
LCI	10.0 (6.0, 17.8)	6.7 (6.0, 7.0)	7.9 (7.4, 10.3)	13.3 (8.3, 17.8)*^
S_{cond}	0.07 ± 0.03	0.04 ± 0.02	0.08 ± 0.02*	0.09 ± 0.03*
S_{acin}	0.14 (0.04, 0.55)	0.08 (0.04, 0.10)	0.10 (0.05, 0.19)	0.30 (0.14, 0.55)*^
LCI_{supine}	9.6 (6.2, 20.2)	6.9 (6.2, 8.3)	9.1 (7.0, 10.6)	14.1 (7.7, 20.2)*^
VDP (%)	14.9 (0.2, 45.0)	2.7 (0.2, 3.3)	4.2 (1.5, 9.2)	29.0 (9.5, 45.0)*^
VH_I (%)	15.1 (6.7, 22.2)	8.9 (6.7, 11.3)	12.1 (9.3, 17.8)	20.1 (15.0, 22.2)*^
Largest defect (%TCV)	3.1 (0.03, 26.8)	0.7 (0.03, 1.3)	1.2 (0.1, 3.5)	15.2 (3.8, 26.8)*^
$N_{defects}$	7 (2, 24)	16 (9, 18)	13 (4, 24)	3 (2, 7)*^

***Table 3**: Ventilation MRI metrics for the 28 patients with images acquired at both end-inspiratory tidal volume (EIVt) and total lung capacity (TLC). Data is presented as median (range). VDP = ventilation defect percentage (%). VH_I = ventilation heterogeneity index. TCV = thoracic cavity volume. * denotes p<0.05 between lung volumes.*

	EIVt	**TLC**
VDP (%)	8.5 (1.5, 45.0)	4.2 (0.2, 35.3)*
VH_I (%)	15.2 (7.4, 22.2)	9.7 (5.7, 18.0)*
Largest defect size (%TCV)	3.3 (0.1, 26.8)	2.0 (0.0, 20.8)*
$N_{defects}$	9 (2, 24)	8.5 (2, 19)
Reversible-volume index		1.1 (1.0, 2.4)
ΔVH_I		-4.1 (-1.5, - 8.3)

Online Supplementary Material
Methods

The MR images were acquired in a 10-12 second breath-hold, during which, both the ventilation image and a ^{1}H anatomical co-registered image were acquired [1]. The end-inspiratory tidal volume (EIVt) scans were always acquired prior to the total lung capacity (TLC) scans, with an interval of 2-5 minutes between. The inhaled bag volumes used for ventilation MRI were titrated based on the patient's standing height. The calculations were based on predicted functional residual capacity (FRC) and TLC volumes in children [2] in an attempt to ensure that children would not be near their TLC when inhaling the EIVt dose. For each height interval of 10cm we calculated the volumes based on the middle of each bracket (i.e. 125cm for the interval 120-130cm). For each height interval we looked at the mean predicted FRC and TLC values. We subtracted 20% off the FRC value to compensate for the effect of posture and then titrated the inhaled bag volume to give a total predicted EIVt volume (FRC + bag volume) of approximately 60% of TLC. The inhaled bag volume consisted of a scaled dose of helium-3 (^{3}He) balanced with nitrogen (N_2). The total bag volume inhaled for TLC was the same as for the EIVt scan but it contained an increased proportion of ^{3}He in order to provide sufficient image signal-to-noise ratio, due to the effect of gas concentration dilution at the higher lung volume. The bag volume height chart can be seen in E-Table 1.

E-Table 4: *Hyperpolarised ^{3}He MR imaging bag volume chart.*

Patient Height	Total Bag Volume	Gas doses	
		EIVt	TLC
160cm +	1.0 L	150 ml ^{3}He + 850 ml N_2	200 ml ^{3}He + 800 ml N_2
150-160cm	800 ml	140 ml ^{3}He + 660 ml N_2	180 ml ^{3}He + 620 ml N_2
140-150cm	650 ml	130 ml ^{3}He + 520 ml N_2	160 ml ^{3}He + 490 ml N_2
130-140cm	500 ml	120 ml ^{3}He + 380 ml N_2	140 ml ^{3}He + 360 ml N_2
120-130cm	400 ml	110 ml ^{3}He + 290 ml N_2	120 ml ^{3}He + 280 ml N_2

Ventilation imaging breathing manoeuvre

In order to deliver the inhaled gas to the patient, the gas was transported in a Tedlar bag (maximum volume = 1.5L), which has a locking ratchet system in place to stop ambient air mixing with the contents. The Tedlar bag had tubing to which a respiratory bacterial filter was placed for the patient to breathe through when required. Prior to performing ventilation imaging the patient was trained on the breathing manoeuvres required. The breathing instructions were given by a respiratory physiologist, specialising in paediatrics.

The instructions were straightforward; the patient was first required to acknowledge that they were ready to proceed before a nose-clip was placed. The patient was then required to gently breathe in and out, at least twice, with each inspiratory and expiratory breath performed at the instructor's request. This ensured that the patient was at a true FRC prior to breathing back in. The instructor assessed this by watching the patient's chest move during respiratory manoeuvres. After the second gentle expiration to FRC, the filter was lowered into the patient's mouth where they were instructed to inhale the full volume of the bag (as soon as the patient began to make an inspiratory effort the release mechanism on the Tedlar back was activated to allow the inhalation of ^{3}He and N_2). For the EIVt image the patient was then instructed to hold their breath for approximately 10 seconds while the image was acquired. For the TLC image, after the full bag volume was inhaled, the filter was immediately removed from the patient's mouth by the instructor and then immediately instructed to take a big breath in to TLC, where they then held their breath for approximately 10 seconds whilst the image was acquired (E-Figure 1).

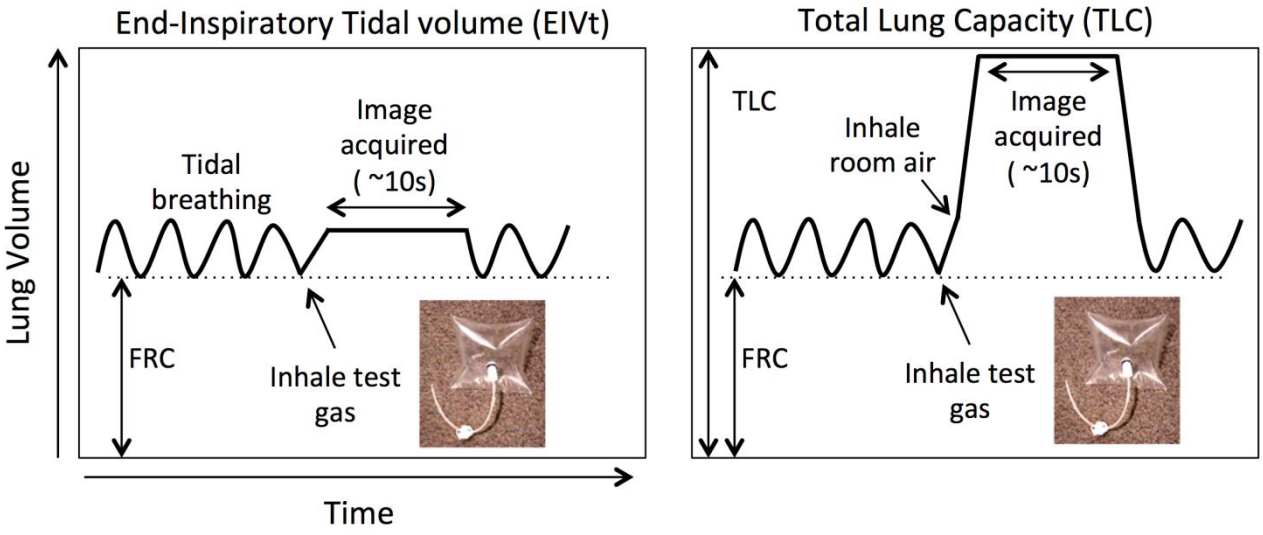

E-Figure 1: *Schematic detailing the breathing sequence performed for both EIVt and TLC ventilation imaging highlighting the difference in the lung volumes for the two MR image acquisitions.*

MR image processing

For both the EIVt and TLC ^{3}He and ^{1}H images, image metrics were calculated from a semi-automated segmentation [3]. The ^{3}He images were segmented in order to calculate the ventilated lung volume (VV) and the ^{1}H images were used to calculate the thoracic cavity volume (TCV). From these two segmentations the ventilation defect percentage (VDP) was defined as the proportion of the TCV without ventilation. The ^{3}He VV segmentation was also utilized to generate a map and histogram distribution of local ventilation heterogeneity, which corresponds to the coefficient of variance of signal intensity from neighbouring ventilated voxels only [4]. From the resulting distribution, the ventilation heterogeneity index (VH_I) was defined as the inter-quartile range of values. The inter-quartile range was reported due to non-normally distributed histograms and best reflects the increased spread of values seen in disease. VH_I for a hypothetical perfectly ventilated lung would be 0, with increasing values representing increased ventilation heterogeneity.

To investigate the size and nature of the distribution of local ventilation defects, a mask of ventilation defects, corresponding to areas of the TCV without ventilation was created, i.e areas contributing to VDP. Contiguous individual ventilation defects were assessed using the software Simplewhere ScanIP (Synopsys, Mountain View, USA). A 3D flood fill algorithm was implemented on this mask to isolate and partition defects. Defects that contributed to less than 1% of total VDP were discarded. The number of remaining defects ($N_{defects}$), as well as the volume of individual defects were calculated. A workflow of image analysis can be found in E-Figure 2.

MRI post-processing workflow

The image workflow analysis can be seen in E-Figure 2, which demonstrates that the ventilation and anatomical images are segmented to create three masks. A ventilation mask, a thoracic cavity mask and a defect mask.

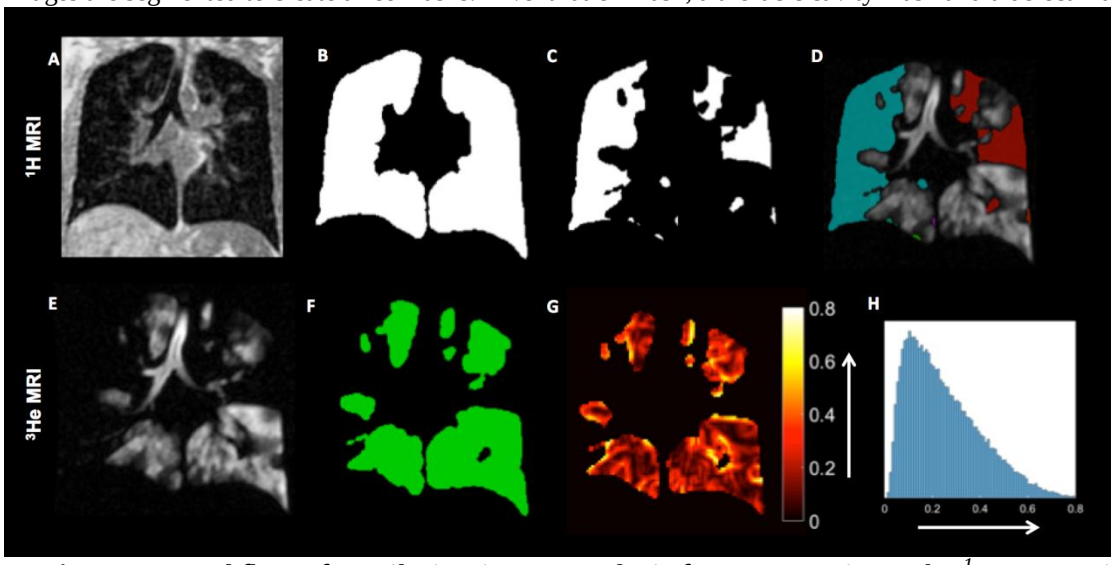

E-Figure 2: *Workflow of ventilation image analysis from one patient. The ^{1}H anatomical image (image A) and the ^{3}He ventilation image (E) are segmented to create a thoracic cavity mask (B) and a ventilation mask (F). Ventilation defect percentage is calculated from the resulting mask volumes. The ventilation defect mask (C) is created as the inverse of the ventilation mask within the thoracic cavity mask (B) and is used to assess the number and volume of contiguous ventilation defects (D). Individual contiguous ventilation defects are shown in different colours in D. The ventilation mask (F) is used to define the area over which the local coefficient of variation is calculated from a 3*3 moving window centred on*

each voxel, before being displayed in a heat map (G) and in histogram form (H). The ventilation heterogeneity index (VH_I) is the inter-quartile range of the local coefficient of variation histogram for the whole lung. Each image or plot (A-H) represents the same coronal central lung slice.

Reversible-volume index

The reversible-volume index is quantitatively derived from the EIVt and TLC ^{3}He and ^{1}H MR images and describes the relative change in ventilated volume when compared to the increase in thoracic cavity volume. The reversible-volume index in a healthy subject with no ventilation defects would equal 1.0, as the increase in ventilated volume would be the same as the increase in thoracic cavity volume when comparing EIVt to TLC images. The reversible-volume index in a patient with non-reversible ventilation defects (resulting from complete obstruction) would also equal 1.0. The reversible-volume index in a subject with CF with significant ventilation defects at EIVt, which at least partially resolve at TLC would have a reversible-volume index >1.0. This is caused by ventilation defects at EIVt becoming ventilated at TLC and therefore the increase in ventilated volume is larger than the increase in thoracic cavity volume. E-Figure 3 gives some worked examples from three patients within this cohort.

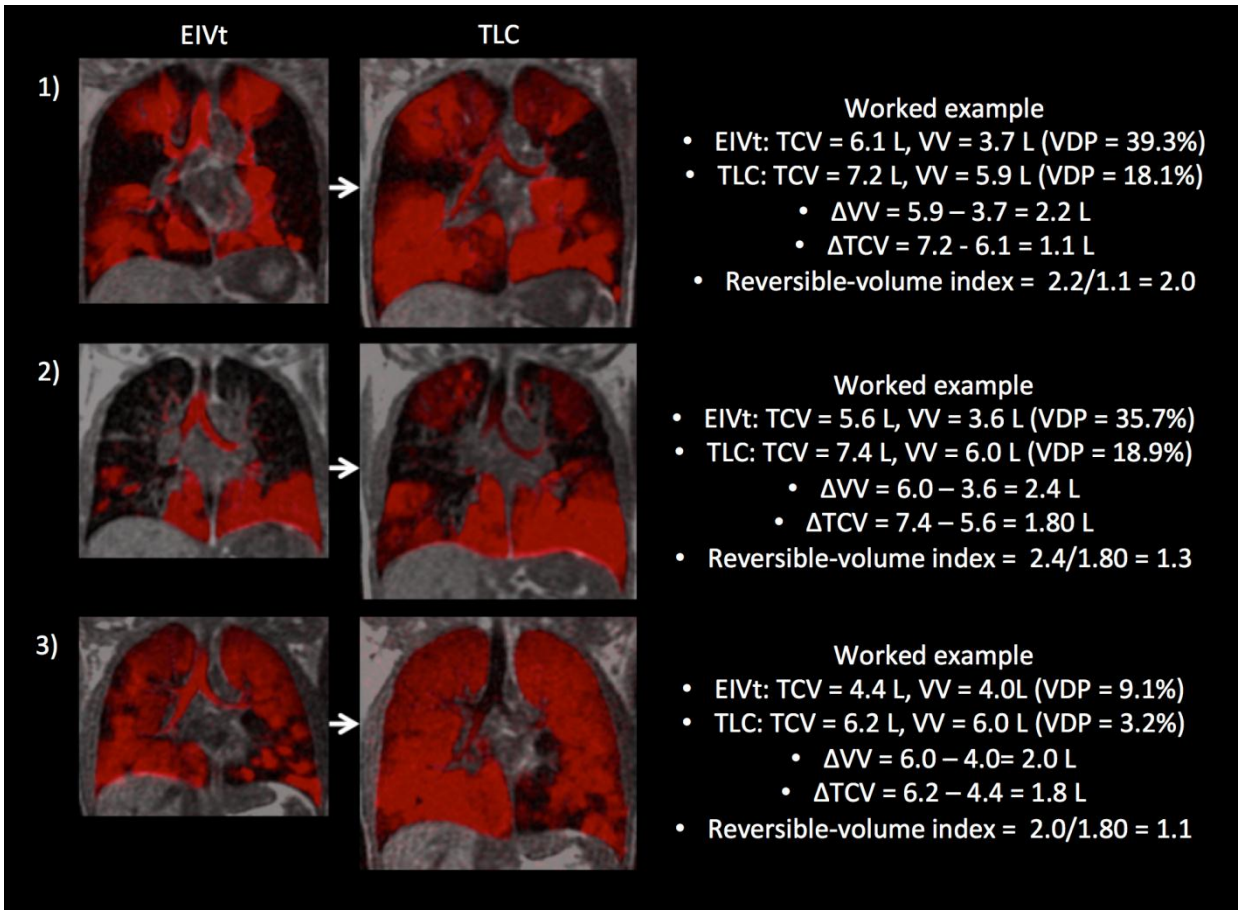

E-Figure 3: *Worked reversible-volume index examples from different patients (1-3) within the study. Representative EIVt and TLC ventilation image slices (red) are overlaid onto the ^{1}H MRI acquired during the same breath-hold (grey). The ventilated volume (VV) is*

calculated from the segmentation of the ^{3}He ventilation image and the thoracic cavity volume (TCV) is calculated from the segmentation of the ^{1}H image. Both the TCV and VV are measured in litres (L).

Results

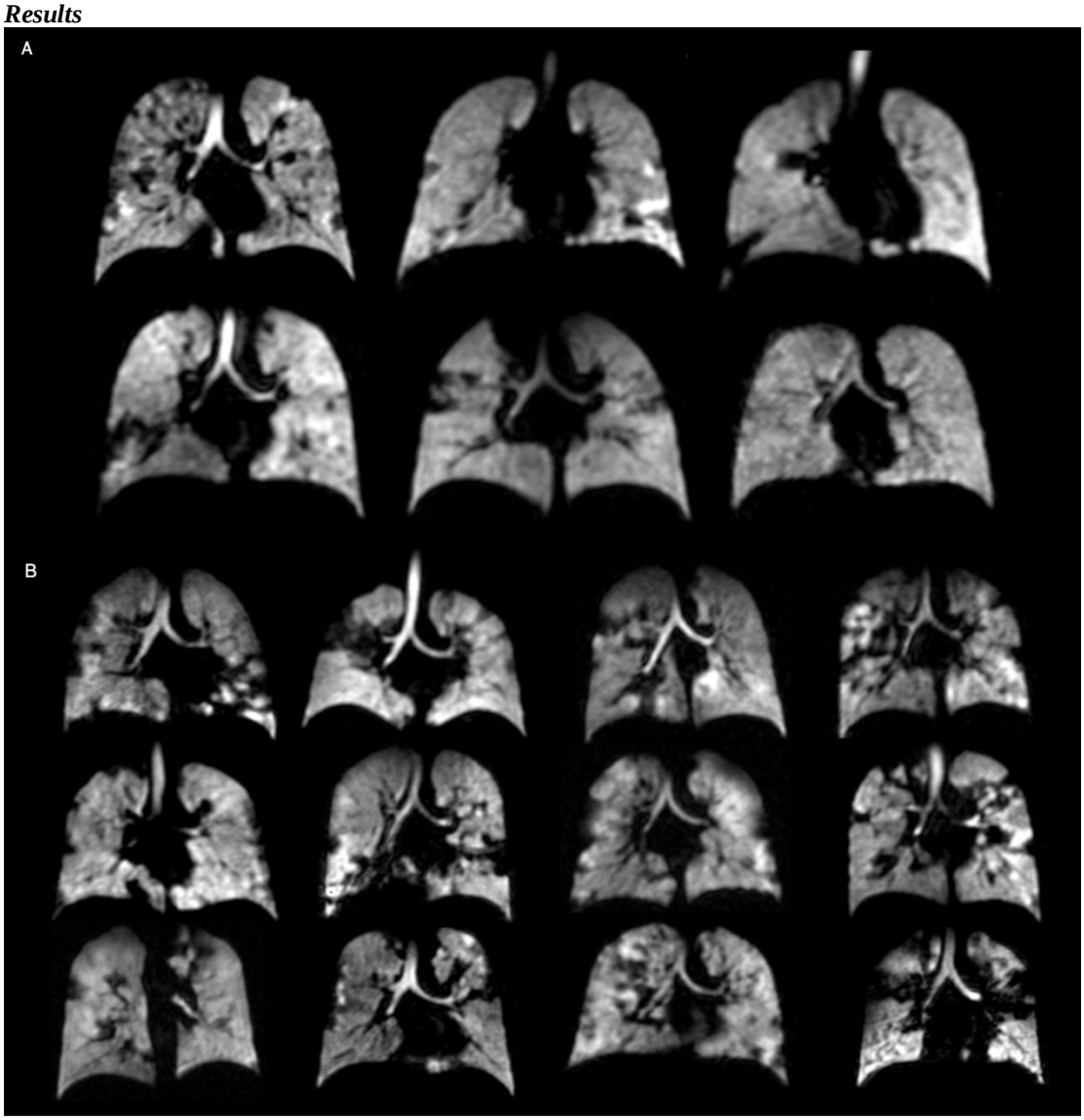

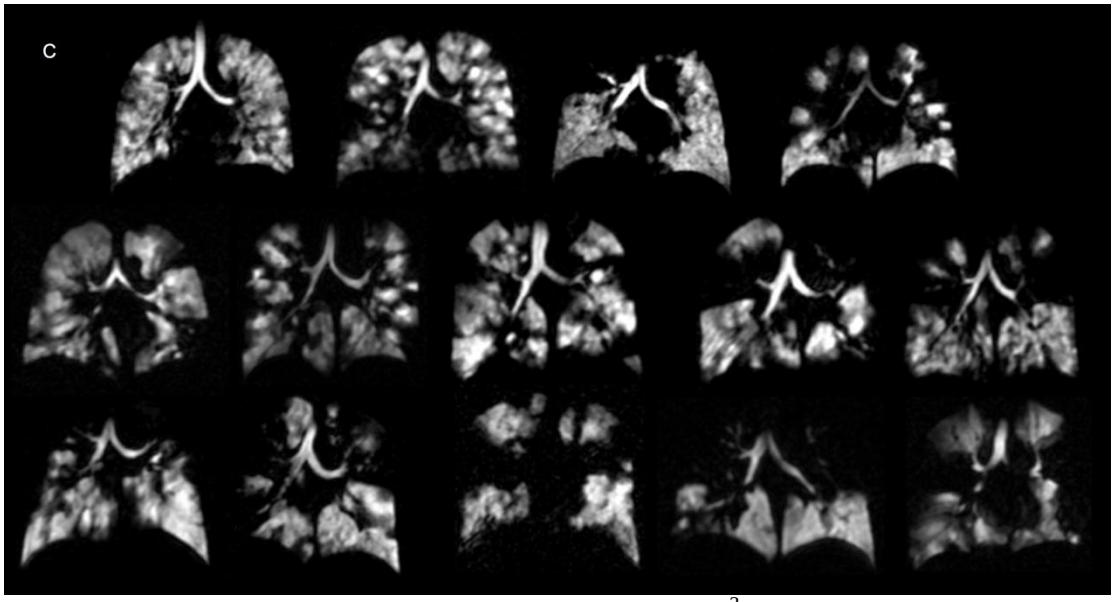

E-Figure 4: *Three panels demonstrating representative ^{3}He ventilation MR images from all CF patients within the study. The first panel (A) is group 1 who have normal FEV_1 and LCI. The second panel (B) is group 2 who have normal FEV_1 but abnormal LCI. The third panel is group 3 (C) who have abnormal FEV_1 and LCI.*

Comparison of seated vs supine MBW data.

Paired t-test analysis of LCI, FRC, S_{cond} and S_{acin} in the seated versus the supine posture was performed as previously described [5]. LCI was significantly lower in the seated position compared to supine (median LCI of 8.4 vs 9.6 respectively, $p<0.001$). FRC was significantly lower supine compared to seated (mean FRC of 1.4 vs 1.8 litres respectively, $p<0.001$). Despite this there was no significant difference for S_{cond} and S_{acin} between postures.

E-Table 5: *Spearman correlations of supine MBW values against ventilation MRI metrics at EIVt. All significant correlations ($p<0.001$) are highlighted by *.*

	LCI	**S_{cond}**	**S_{acin}**
VDP (%)	0.83*	-0.003	0.8*
VH_I (%)	0.80*	0.17	0.75*
Largest defect (%TCV)	0.80*	-0.02	0.75*
$N_{defects}$	-0.66*	0.14	-0.65*
Reversible-volume index	0.78*	-0.15	0.76*
ΔVH_I	0.22	0.28	0.35

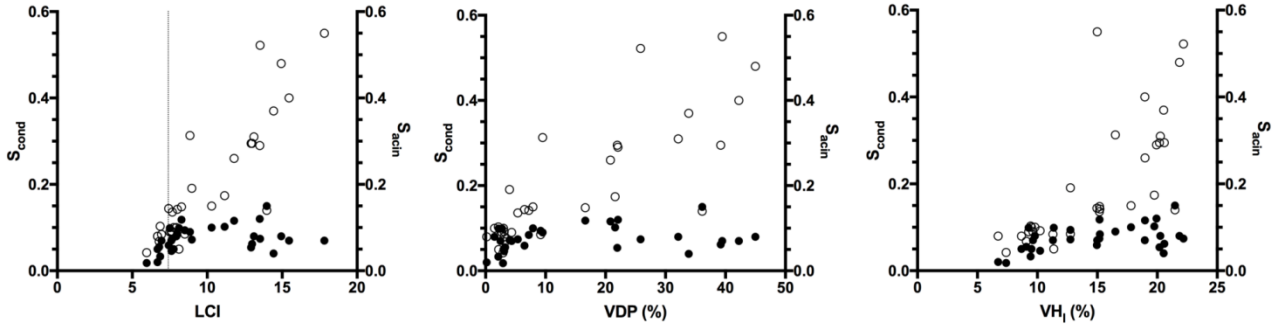

E-Figure 5: *Scatterplots of S_{acin} (open circles, right Y axis) and S_{cond} (closed circles, left Y axis) against; LCI (dashed line indicates the upper limit of normal), VDP and VH_I. S_{cond} consistently demonstrates a plateau effect with increased levels of disease severity, without evidence of statistical correlation. S_{acin} however demonstrates significant correlations with LCI (r=0.86), VDP (r=0.84) and VH_I (r=0.82).*

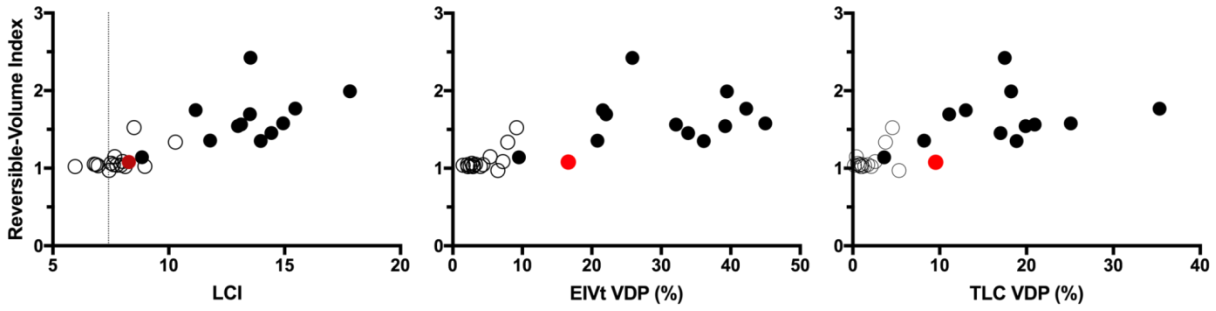

E-Figure 6: *Spearman correlation of LCI and VDP at both EIVt and TLC, against the reversible-volume index. The data has been segregated to visualise two groups, those with an* $FEV_1 \leq$ *-1.64 (closed circles) and those with an* $FEV_1 >$ *-1.64 (open circles). Dashed line represents the LCI upper limit of normal. There is a strong correlation between the reversible-volume index and both LCI (r=0.82) and VDP at both lung volumes (r=0.85 at EIVt and r=0.75 at TLC) (p<0.001). The data points highlighted by a red circle represent a patient with a low reversible-volume index, but relatively large values for VDP. Images for this patient are shown in E-Figure 7.*

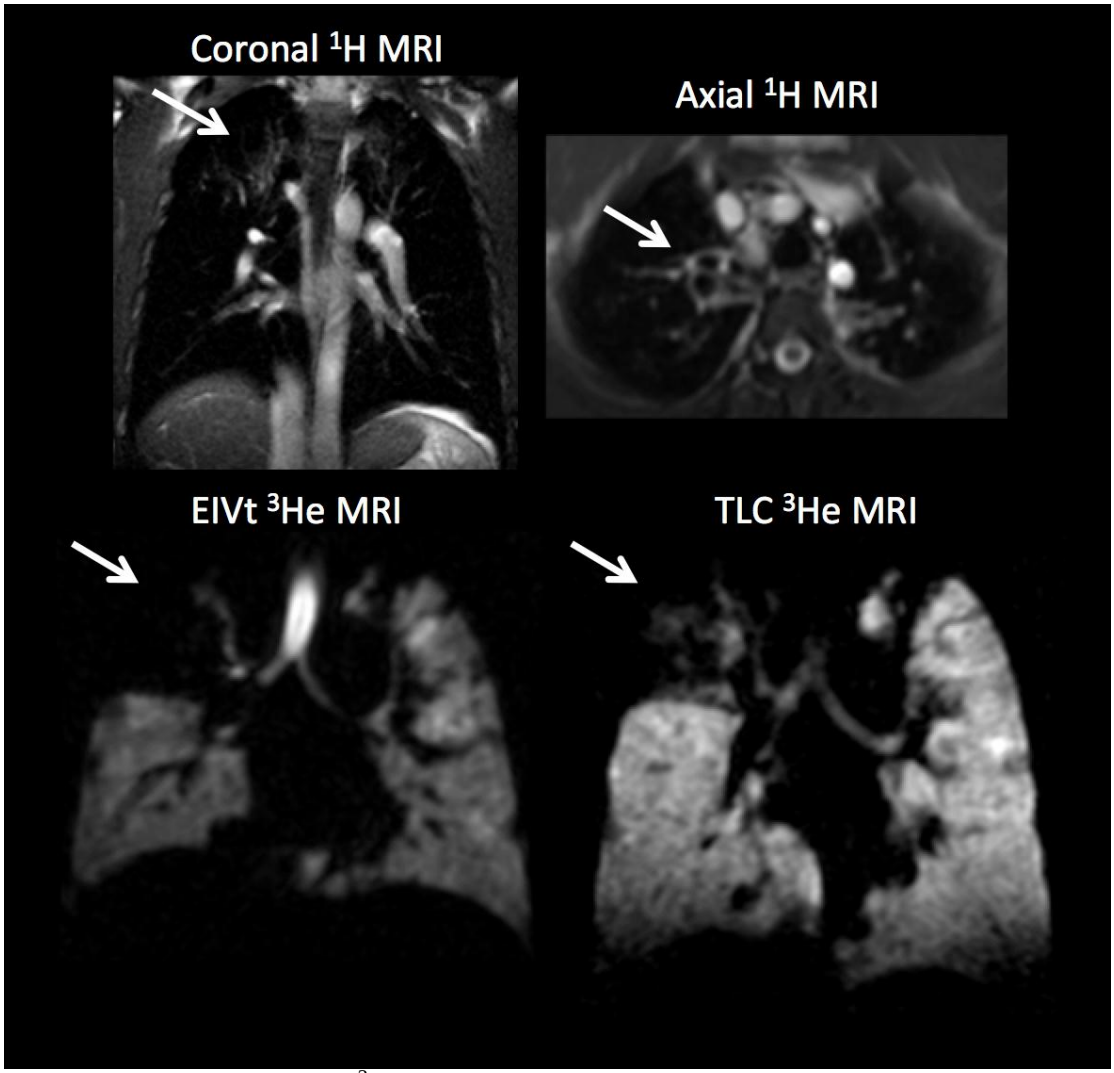

E-Figure 7: *EIVt and TLC* ^{3}*He comparison for a patient with CF and representative* ^{1}*H anatomical MR imaging demonstrating bronchiectasis. At EIVt this patient has a large ventilation defect in the right upper lobe (defect size = 10 %TCV, total VDP =*

16.6%), which is in the same area as the anatomical abnormalities. At TLC, this ventilation defect only achieves a small amount of ventilation and reduces in volume by 103ml (defect size = 5.7 %TCV, total VDP = 9.5%). As a result this subject has a low reversible-volume index of 1.1. This patient however has an arguably lower than anticipated LCI of 8.3, when compared to the FEV_1 z-score of -3.1. These data suggest that the low LCI is due to this large defect being almost completely obstructed and therefore not contributing to ventilation during MBW.

References

1. Horn, F.C., B.A. Tahir, N.J. Stewart, G.J. Collier, G. Norquay, G. Leung, R.H. Ireland, J. Parra-Robles, H. Marshall, and J.M. Wild, *Lung ventilation volumetry with same-breath acquisition of hyperpolarized gas and proton MRI.* NMR Biomed, 2014. **27**(12): p. 1461-7.
2. Rosenthal, M., D. Cramer, S.H. Bain, D. Denison, A. Bush, and J.O. Warner, *Lung function in white children aged 4 to 19 years: II--Single breath analysis and plethysmography.* Thorax, 1993. **48**(8): p. 803-8.
3. Hughes, P.J.C., F.C. Horn, G.J. Collier, A. Biancardi, H. Marshall, and J.M. Wild, *Spatial fuzzy c-means thresholding for semiautomated calculation of percentage lung ventilated volume from hyperpolarized gas and (1) H MRI.* J Magn Reson Imaging, 2018. **47**(3): p. 640-646.
4. Tzeng, Y.S., K. Lutchen, and M. Albert, *The difference in ventilation heterogeneity between asthmatic and healthy subjects quantified using hyperpolarized 3He MRI.* J Appl Physiol (1985), 2009. **106**(3): p. 813-22.
5. Smith, L.J., K.A. Macleod, G.J. Collier, F.C. Horn, H. Sheridan, I. Aldag, C.J. Taylor, S. Cunningham, J.M. Wild, and A. Horsley, *Supine posture changes lung volumes and increases ventilation heterogeneity in cystic fibrosis.* PLoS One, 2017. **12**(11): p. e0188275.